Nanoscale

PAPER



Cite this: *Nanoscale*, 2022, **14**, 10531

# *In vitro* and *ex vivo* nano-enabled immunomodulation by the protein corona†

Francesca Giulimondi,‡[a] Luca Digiacomo,‡[a] Elisabetta Vulpis,[a] Luisa Loconte,[a] Gianmarco Ferri,[b] Francesco Cardarelli,[b] Daniela Pozzi,[a] Alessandra Zingoni[a] and Giulio Caracciolo *[a]

Received 5th April 2022,
Accepted 1st July 2022

DOI: 10.1039/d2nr01878k

rsc.li/nanoscale

New technologies with the capacity to tune immune system activity are highly desired in clinical practice and disease management. Here we demonstrate that nanoparticles with a protein corona enriched with gelsolin (GSN), an abundant plasma protein that acts as a modulator of immune responses, are avidly captured by human monocytic THP-1 cells *in vitro* and by leukocyte subpopulations derived from healthy donors *ex vivo*. In human monocytes, GSN modulates the production of tumor necrosis factor alpha (TNF-α) in an inverse dose-dependent manner. Overall, our results suggest that artificial coronas can be exploited to finely tune the immune response, opening new approaches for the prevention and treatment of diseases.

To date, clinical applications of conventional nano-delivery systems such as nanoparticles (NPs) are generally associated with several drawbacks, including the off-target release of their payload[1] and rapid NP clearance from the systemic circulation.[2] Indeed, once injected into the bloodstream, NPs are usually recognized as potential pathogens, as "nonself" antigens, triggering processes that protect the host organism against foreign agents.[3] Molecular recognition and direct interactions between NPs and immune cells strongly depend on the NPs' physicochemical features (*e.g.*, size,[4] shape,[5] and electric charge[6,7]) and especially their surface properties.[8–10] Thus, the biomolecular/protein corona (PC), *i.e.*, an evolving layer formed at the surface of NPs upon contact with biological fluids and composed of biomolecules (mostly proteins), is the main interface that mediates NP–immune system interactions.[11,12]

Although there is not yet general consensus regarding differential immune stimuli dependence on the PC, recent evidence suggests that the PC can either stimulate[8] or elude[13,14] the immune system, acting on innate immune cell activity, complement cascade,[15] and adaptive immune response.[3] Therefore, the PC could be employed to modulate immune responses at different levels. This in turn may represent a possible method for tuning the immune response to a particular clinical goal, *i.e.*, enabling prolonged circulation of targeted nanomedicines or, conversely, activating tumor-associated immune cells for nano-immunotherapies.

Some promising strategies rely on pre-coating NPs with an artificial PC[13–16] that, in turn, regulates interactions with the desired cells and the translocation of NPs across biological barriers. Artificial PCs have been created for targeting applications (*e.g.*, brain tissue[17,18]) and they often depend on non-covalent NP functionalization with single proteins, as it has recently been demonstrated that non-covalent binding of the desired ligands is more effective than other kinds of conjugations.[16] Our nanoplatform for hosting the artificial PC is a cationic liposome (CL), since liposomes may function as potentiation agents of the immune response by carrying antigens and immunomodulatory molecules.[19,20] Indeed, the reconstitution of antigens into liposomal membranes, or their incorporation into the inner hydrophilic core, has been reported to enhance macrophage activation,[21] antibody production,[22] and effective induction of cellular cytotoxicity.[23] To this end, we chose 1,2-dioleoyl-3-trimethylammonium-propane (DOTAP) which is one of the most popular and widely used cationic lipids for gene transfection applications.[24] Among the identified possible immunostimulant proteins, we selected plasma gelsolin (GSN) as it is a highly conserved abundant circulating plasma protein involved in manifold physiological processes, such as macrophage activation,[25] regulation of macrophage-mediated host defence functions, and alteration of the expression of inflammatory cytokines.[26] Furthermore, plasma GSN can bind to several cellular lipids such as lysopho-

[a]*Department of Molecular Medicine, "Sapienza" University of Rome, Viale Regina Elena 291, 00161 Rome, Italy. E-mail: alessandra.zingoni@uniroma1.it, giulio.caracciolo@uniroma1.it*

[b]*Laboratorio NEST, Scuola Normale Superiore, Piazza San Silvestro 12, 56127 Pisa, Italy. E-mail: gianmarco.ferri@sns.it, francesco.cardarelli@sns.it*

†Electronic supplementary information (ESI) available. See DOI: **https://doi.org/10.1039/d2nr01878k**

‡These authors contributed equally to this work.

sphatic acid and phosphatidylinositol acting as mediators of inflammatory responses[27] and modulators of acute innate immune responses.[28] Here, immunomodulation induced by artificial GSN-enriched coronas was explored both *in vitro* and *ex vivo* (Fig. 1). As a first step, DOTAP-GSN complexes with different synthetic identities (*i.e.*, size and zeta-potential) and GNS surface densities were prepared by bulk mixing of DOTAP and GSN and tuning the GSN/DOTAP weight ratio. Next, we investigated the capture of DOTAP-GSN complexes using human monocytic THP-1 cells *in vitro* and demonstrated that particle internalization positively correlates with the GNS density at the particle surface. Experimental *in vitro* validation is an established paradigm for testing the immunomodulatory effects of nanomaterials, but the usage of *in vitro* data to predict *ex vivo*/*in vivo* phenomena has been frequently questioned.[29] According to our present understanding,[30,31] the discrepancy between *in vitro* and *ex vivo*/*in vivo* data is due to our limited knowledge of the nano–bio-interactions between nanomaterials and biological systems. Upon *ex vivo*/*in vivo* administration, plasma proteins bind to nanomaterials and endow them with a new biological identity that controls their physiological response. To mimic physiological conditions, we incubated DOTAP and DOTAP-GSN complexes in human plasma (HP) and, subsequently, we exposed DOTAP/HP and DOTAP-GSN/HP complexes to leukocyte subpopulations derived from healthy donors *ex vivo*. DOTAP-GSN/HP complexes were more avidly internalized by leukocyte subpopulations as compared with DOTAP/HP with no precise dependence on the GNS surface density. On the other hand, in human monocytes, GSN modulated the production of tumor necrosis factor alpha (TNFα) in an inverse dose-dependent manner.

## Results and discussion

Preliminary dynamic light scattering (DLS) experiments were aimed at characterizing the size and zeta-potential of DOTAP. The size distribution of uncoated DOTAP was unimodal and centered at 129 ± 3 nm. The corresponding zeta-potential was highly positive with a distribution centered at 55 ± 3.9 mV. We prepared DOTAP/GSN complexes with different GNS surface

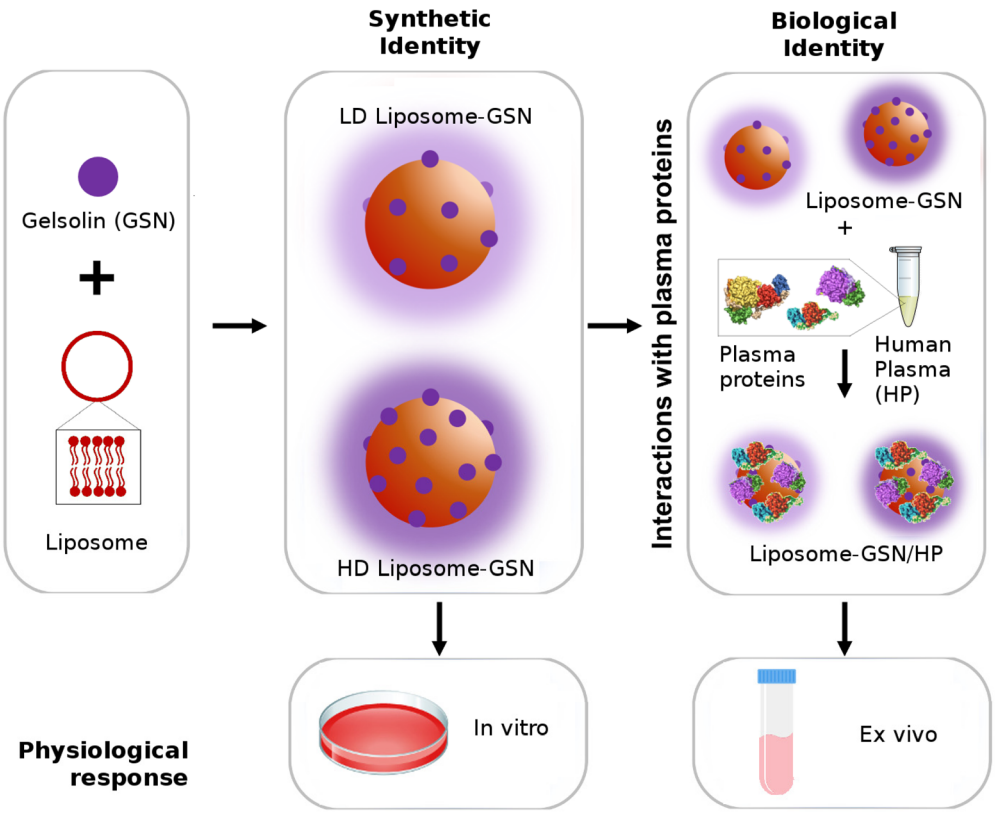


**Fig. 1** Exposing liposomes to human gelsolin (GSN) leads to GSN-coated liposomes. Fine-tuning of the GSN/lipid weight ratio generates liposomes with low-density (LD) and high-density (HD) coatings. *In vitro* validation under serum-free conditions is an established paradigm for testing the immunomodulatory effects of nanomaterials with a precise synthetic identity. This condition was tested by administration of LD and HD liposome–GSN to human monocytic the THP-1 cell line *in vitro*. Over the last 15 years, we have started to understand that the synthetic identity that nanomaterials possess *in vitro* could be very different from the biological identity acquired upon interaction with a biological fluid. In human plasma (HP), liposome–GSN complexes acquire a novel "biological identity" due to the protein adsorption and consequent formation of a protein corona. The impact of biological identity on the physiological response was evaluated by the administration of liposome–GSN/HP complexes to leukocyte subpopulations derived from healthy people (*ex vivo*).

densities by incubating cationic DOTAP with anionic GSN at 8 GSN/DOTAP weight ratios for 15 min at 37 °C. The electrostatic interaction between cationic NPs and anionic biomolecules has been extensively used in the literature.[32] Surface decoration reduces the inter-particle repulsive barrier causing aggregation and size increase. Exposing cationic liposomes to a single protein solution may lead to the formation of liposome–protein complexes with positive, neutral, or negative surface charges, depending on two main factors, *i.e.*, the protein isoelectric point (PI) and the protein/lipid molar ratio. As GSN carries a slightly negative charge at physiological pH (nominal pI = 6.2), the surface properties of DOTAP-GSN complexes could be tuned by adjusting the GSN/DOTAP weight ratio. We, therefore, validated the presence of GSN at the lipid surface by measuring the zeta potential and the size of DOTAP/GSN complexes. Results are presented in Fig. S1 in the ESI.† The coating data were divided into two groups: low-density decoration (LD) (for GSN/DOTAP weight ratio < 0.2) and high-density decoration (HD) (for GSN/DOTAP weight ratio > 0.2). According to the considerations made in Fig. S1 in the ESI,† we chose GSN/DOTAP weight ratios equal to 0.1 and 4 as LD and HD complexes, respectively. Then, we accessed the coating of DOTAP-GSN complexes by one-dimensional sodium dodecyl sulfate-polyacrylamide gel electrophoresis (1D SDS-PAGE). A gel image is shown in Fig. S2 in the ESI.† To this end, GSN was isolated from DOTAP according to the optimized protocols[33] and loaded in the wells of the gel. Protein profiles shown in Fig. S2† were analyzed by custom-made scripts and the molecular weight (MW) distributions are shown in Fig. 2a.

The MW profiles of LD and HD DOTAP-GSN complexes exhibited a single band at 88 kDa that is fully compatible with the nominal MW of GSN (86 kDa). The 1D intensity profiles were not normalized, *i.e.*, the curves represent the detected lane intensity. Going from the LD to HD the abundance of GSN in the artificial corona increased according to the characterization results reported in Fig. S1.†

At this point, we investigated the interaction of DOTAP-GSN complexes with immune system cell components *in vitro*. Macrophages defend against infections and foreign pathogens, and their interaction with NPs may determine NP-enabled immunomodulation.[34] For traditional cancer therapy, nonspecific uptake by immune cells has been considered detrimental as it reduces the drug availability at the tumor tissue.[35–37] On the other side, massive capture by innate immune cells, such as monocytes, macrophages, and dendritic cells *in vivo*, has been recently exploited to enhance the accumulation of NPs in tumours.[38] For instance, some liposomal drugs are designed to target perivascular tumour-associated macrophages (TAMs) that accumulate in the tumour tissue.[39] To assess NP uptake, DOTAP, LD DOTAP-GSN, and HD DOTAP-GSN complexes were incubated with human monocytic THP-1 cells in a serum-free medium for 3 h. This cell line was chosen as it has become a popular model to estimate the modulation of monocyte and macrophage activities.[40] The lipid dose/well was chosen according to the results of preliminary cell viability experiments reported in Fig. S3 in the ESI.† Flow cytometry was used to quantitatively assess uptake by THP-1 cells at four time points: 30 min, 60 min, 120 min, and 180 min post-administration. Particle internalization, expressed in terms of cell percentage, was in the following order: DOTAP ~ LD DOTAP-GSN < HD DOTAP-GSN. (Fig. 3a). Confocal microscopy imaging of NP uptake by THP-1 shown in Fig. 3b indicated that significantly much more HD DOTAP-GSN was internalized as compared to DOTAP. Calculation of the number of complexes per cell (Fig. 3c) showed that the GSN corona had a major effect on NP uptake.

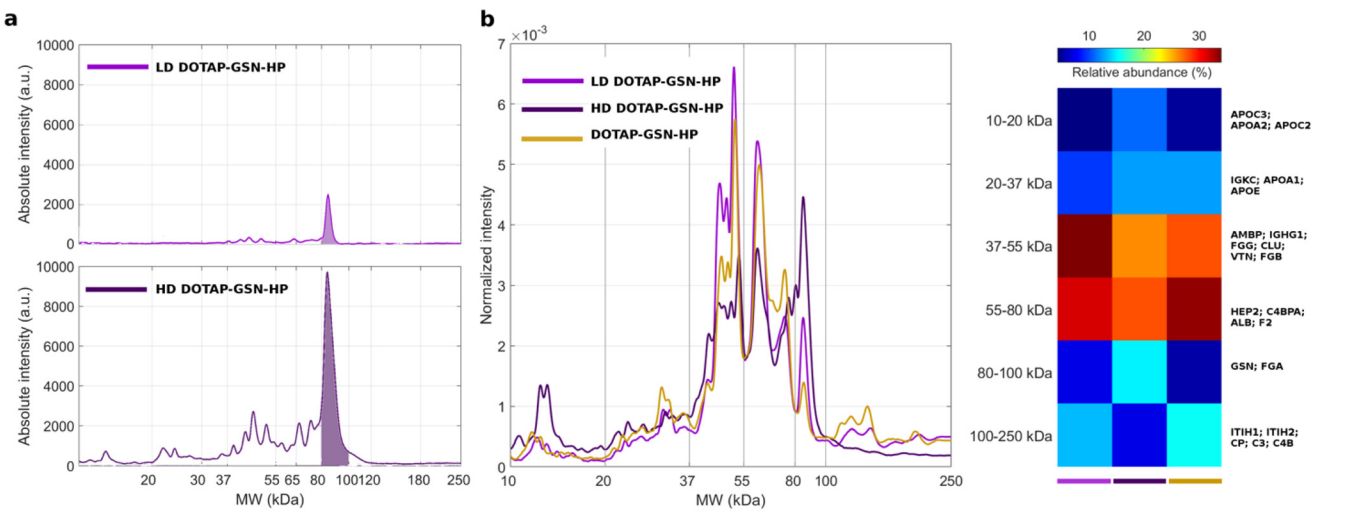


**Fig. 2** Synthetic (a) and biological identities (b) of liposome–GSN complexes. The coating of DOTAP-GSN complexes was characterized by densitometry analysis of the one-dimensional (1D) SDS-PAGE image reported in Fig. S1 in the ESI.† (a) 1D molecular weight distribution of LD DOTAP-GSN and HD DOTAP-GSN. (b) 1D molecular weight distribution of DOTAP/HP complexes and LD DOTAP-GSN/HP and HD DOTAP-GSN/HP complexes. Heat map of the most abundant proteins detected in the protein corona of LD DOTAP-GSN/HP, HD DOTAP-GSN/HP, and DOTAP/HP determined by tandem mass spectrometry.

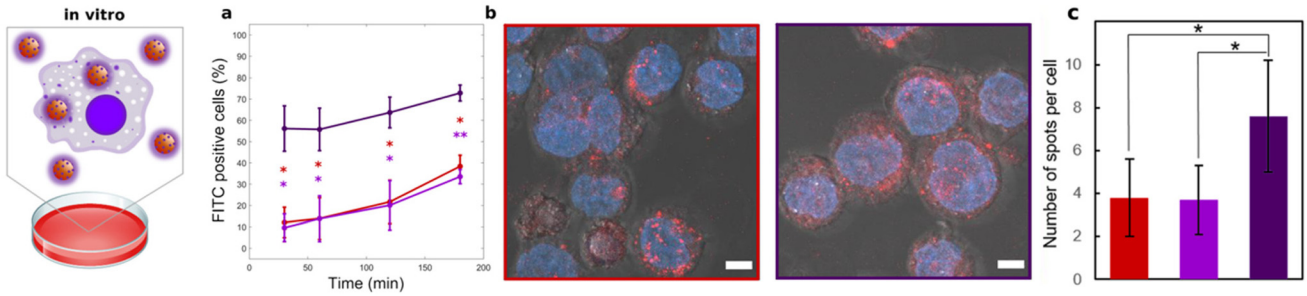


**Fig. 3** (a) Flow cytometry measurements for DOTAP (red points), LD DOTAP-GSN (light purple), and HD DOTAP-GSN (deep purple) upon incubation with human monocytic THP-1 cells. Results are reported as the percentage of FITC-positive cells. Differences between DOTAP and LD DOTAP-GSN were not significant. For DOTAP and LD DOTAP-GSN, statistical significance was evaluated with respect to HD DOTAP-GSN (red and light purple asterisks, respectively) using Student's *t*-test (*$p < 0.05$; ** $p < 0.01$). (b) Representative confocal microscopy images of human monocytic THP-1 cells incubated with DOTAP (red framework) and HD DOTAP-GSN (deep purple framework). (c) Calculation of the number of complexes per cell shows that the artificial protein corona composed of GSN has a major effect on NP uptake. Scale bars of confocal images are 5 μm. Statistical significance was evaluated using Student's *t*-test (*$p < 0.05$).

As clarified above, we chose GSN as a model artificial PC for being a highly conserved abundant plasma protein and for its ability to work as a strong immunomodulator. According to our expectations, a GSN-enriched PC can promote massive uptake by macrophages. However, the specific macrophages' receptors involved in the molecular recognition of GSN motifs are currently unknown. For this reason, we could not explore the exact mechanism of NP internalization in depth. For the sake of completeness, we discuss some non-specific factors that might contribute to explaining flow cytometry and confocal microscopy in the ESI.†

Decorating NPs with single proteins (*e.g.*, HSA[41] and transferrin[42]) could enable controlled interactions with living systems. Nevertheless, the surface of decorated NPs may be strongly modified by protein adsorption in physiological environments. Based on the current literature,[43–47] an adduct must be evaluated in terms of the PC attracted upon interaction with the biological milieu, as that interface will trigger the physiological response. To reproduce the interface acquired by DOTAP and DOTAP-GSN *in vivo*, we exposed them to HP for 1-hour at 37 °C. DOTAP/HP complexes exhibited small size (163 ± 14 nm) and negative zeta potential (−22 mV) (Table S1 in the ESI†). Inversion of the zeta potential produced by HP (from 55 mV to −22.1 ± 1.3 mV) is a well-known behaviour for several NP types embedded in HP[48] and indicates complete coating of the liposome surface with plasma biomolecules. The size of LD DOTAP-GSN/HP complexes slightly increased (182 ± 7 nm) and the zeta-potential reversed to negative values (zeta potential ∼ −28 ± 4 mV). On the other hand, HD DOTAP-GSN complexes underwent massive disaggregation leading to re-entrant condensation[49] and promoting the formation of negatively-charged particles (zeta potential ∼ −13 ± 3.5 mV) with decreasing size (318 ± 14 nm). Exposure of DOTAP and DOTAP-GSN complexes to HP elicited peculiar protein patterns (Fig. 2b) due to the enrichment by manifold different plasma proteins. The protein profiles of LD and HD DOTAP-GSN/HP complexes resembled those of DOTAP/HP with a degree of similarity in the order of LD > HD. Previous studies have shown that the composition of the PC varies due to the balance between protein abundance and affinity to the particle surface.[30,50] Our findings suggest that plasma proteins preferentially bind to the free lipid surface (*i.e.*, not coated by GSN) with GSN molecules remaining bound to lipid membranes. The composition of the PC was further assessed by nano liquid chromatography tandem mass spectrometry (nano-LC MS/MS). To visualize changes in the protein patterns, the identified proteins were grouped into five regions of the MW and shown in a heat map (Fig. 2b). Among the identified proteins, the most abundant ones were apolipoproteins, immunoglobulins, complement proteins, serum albumin, clusterin, fibrinogen, and vitronectin. Nano-LC MS/MS also confirmed that DOTAP-GSN/HP complexes were enriched with GSN in the order of HD > LD.

The following step was assessing the particle uptake by different leukocyte subpopulations derived from peripheral blood mononuclear cells (PBMCs) of healthy subjects *ex vivo*. DOTAP/HP, LD DOTAP-GSN/HP, and HD DOTAP-GSN/HP were injected into the donor's whole blood and sequestration by circulating leukocytes was measured over time (Fig. S4 in the ESI†) using a strategy recently reported[51] (experimental settings can be found in Fig. S5 in the ESI†). Circulating leukocytes are immune system cells that contribute to defending the body against both infectious diseases and foreign invaders. They act as a major barrier to NP-mediated drug delivery *in vivo*.[2] Pre-coating DOTAP liposomes with HP (gold histograms) could avoid their capture by circulating leukocytes in all the investigated populations. DOTAP-GSN/HP complexes were massively internalized by almost all the studied populations, with an increasing trend over time (Fig. S4 in the ESI†), until plateau values were reached. In Fig. 4 we report leukocyte capture for the longest exposure time (*i.e.*, $t$ = 1-hour).

B lymphocytes (*i.e.*, CD19+), monocytes (*i.e.*, CD14+ CD3−), and granulocytes showed the highest uptake (between 80%

 

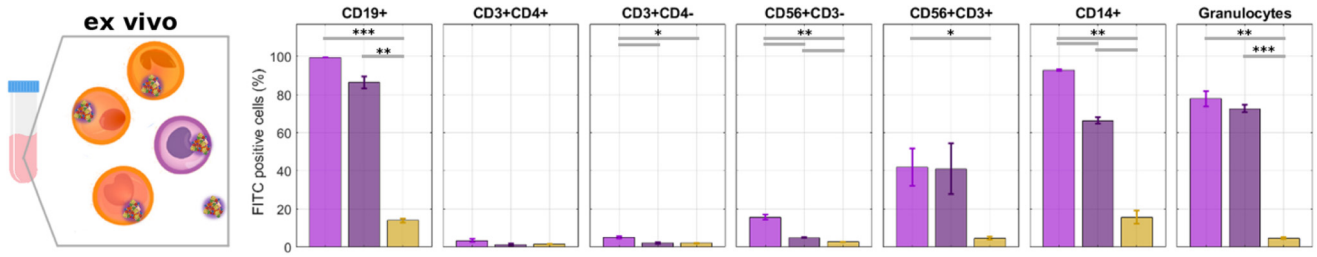


**Fig. 4** Leukocyte uptake of DOTAP/HP (yellow), LD DOTAP-GSN/HP (deep purple), and HD DOTAP-GSN/HP (light purple) in whole blood. The fluorescence signal of internalized nanoparticles was measured as the percentage of FITC-positive cells by gating on distinct leukocyte subpopulations. Data analysis was performed using FlowJo software, with results reported as the mean ± standard deviation of three healthy donors. The statistical significance of differences between DOTAP/HP and LD DOTAP-GSN or HD DOTAP-GSN/HP is reported as the *p*-value from Student's *t*-test (* $p < 0.05$; ** $p < 0.01$; *** $p < 0.001$).

and 94%), whereas NK (CD56+CD3−) and NKT (CD56+CD3+) cells present a lower level of uptake (between 18% to 40%) and finally negligible capture was observed in T lymphocytes (*i.e.*, CD3+CD4+ and CD3+CD4−). As expected, immune cells having a phagocyte activity like monocytes and granulocytes show a higher capability to uptake DOTAP-GSN/HP complexes. In addition, it is interesting to note that B lymphocytes are also efficient to capture DOTAP-GSN/HP complexes and this observation might be relevant to the design of DOTAP-protein complexes used as vaccines able to boost either humoral or cell-mediated adaptive immunity since B lymphocytes act as antigen presenting cells to T helper lymphocytes.

As GSN was chosen to promote interaction with immune cells, the positive correlation between GSN enrichment and capture by circulating leukocytes confirmed our expectations.

We finally investigated whether the uptake of DOTAP-GSN by $CD14^+$ monocytes corresponded to a functional biological effect. We decided to evaluate the production of tumour necrosis factor alpha (TNFα) since it represents a proinflammatory cytokine that reflects the activation status of monocytes and importantly previous findings showed that GSN can inhibit the production of TNFα in pregnant women[27] and mice.[52] To this aim, leukocytes were purified from the peripheral blood of healthy donors and incubated for 1 hour at 37 °C with DOTAP, DOTAP/HP, and DOTAP-GSN/HP complexes. BFA was added to the culture medium and left for additional 3 hours to allow cytokine intracellular accumulation. The results reported in Fig. 5 revealed that HD DOTAP-GSN/HP inhibited TNFα production with respect to DOTAP/HP and LD DOTAP-GSN/HP.

These findings prompted us to conclude that the large amount of GSN enriching the PC of HD DOTAP-GSN/HP might inhibit the production of TNFα naturally produced by DOTAP-protein complexes.

Many studies have provided evidence that toll-like receptors (TLRs) play a pivotal role in monocyte/macrophage-mediated proinflammatory cytokine production. Thus, we checked whether some TLRs could contribute to the TNFa production in response to DOTAP-protein complexes. We focus our attention on TLR2 and TLR4 since they bind not only pathogen-derived components but also host-derived molecules.[53] To this

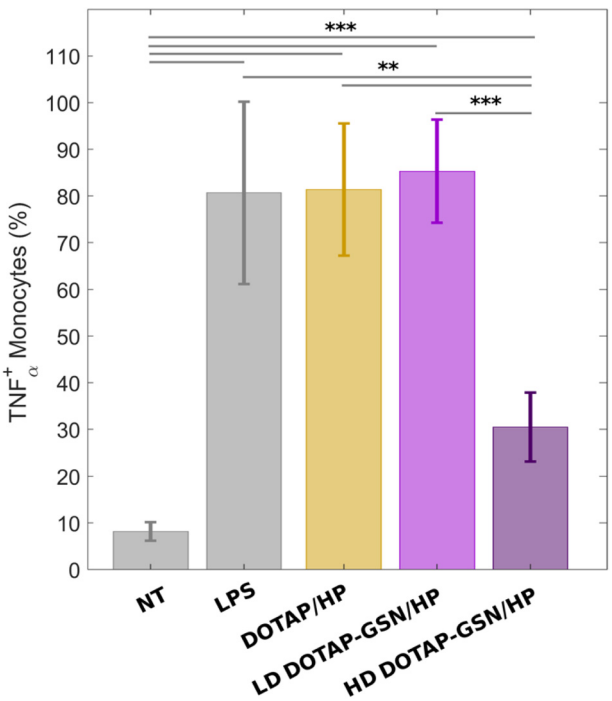


**Fig. 5** TNFα production by monocytes in response to DOTAP/HP, LD DOTAP-GSN/HP, and HD DOTAP-GSN/HP. PBMCs were treated with the indicated NPs for 1 hour at 37 °C. BFA was added to the culture medium and left for additional 3 hours. Intracellular TNFα detection was measured by immunofluorescence and FACS analyses and reported as the percentage of $TNF\alpha^+$ $CD14^+$ cells. Non-treated cells (N.T.) and LPS were used as the negative control and positive control, respectively. Statistical significance was evaluated using Student's *t*-test (* $p < 0.05$; ** $p < 0.01$; *** $p < 0.001$).

aim, we used a 293-derived reporter cell line engineered to co-express TLR2 or TLR4 along with an NF-kB-driven luciferase reporter. As shown in Fig. S6,† exposure to specific TLR agonists induced luciferase activity in the TLR2 and TLR4 reporter cell lines, whereas no effect was observed in the presence of DOTAP/HP or DOTAP-GSN/HP complexes, thus indicating that other receptor–ligand pairs contributed to the observed TNFα production.

## Conclusions

In summary, we present the design and development of artificial GSN coronas capable of triggering the activation of immune response in terms of cellular uptake and modulating pro-inflammatory cytokine production. An artificial PC may allow a controlled interaction with immune system cells, causing immune blinding or immune activation. Since DOTAP/HP escapes capture by THP-1 cells and circulating leukocytes, it shows great promise for the targeted delivery of nanomedicines to non-immune cells (including tumor cells). On the other hand, DOTAP-GSN/HP shows a massive uptake by immune system cells and retains the capability to trigger the production of TNFα by monocytes depending on the GSN density at the particle surface. We envision that deeper investigation may contribute to the development of artificial PC systems to control and predict the interaction of NPs with the immune system. This approach could optimize donor-specific and tissue-specific deliveries and minimize potential adverse effects.

## Experimental details

### Chemicals

1,2-Dioleoyl-3-trimethylammonium propane (DOTAP) was purchased from Avanti Polar Lipids (Alabaster, AL), and the corresponding liposomal formulation (concentration 1 mg $mL^{-1}$) was prepared by lipid film hydration followed by mechanical extrusion (details of these established protocols can be found elsewhere[9]). For flow cytometry experiments, liposomes were labeled with 7-nitrobenzofurazan (hereafter referred to as NBD-labeled liposomes). Gelsolin (product: G8032) was purchased from Sigma Aldrich (St Louis, MI, USA). HP (product: P9523) was purchased from Sigma Aldrich. Plasma powder was reconstituted to the volume indicated on the label with Milli-Q® $H_2O$ (Merck, USA).

### Preparation of liposome and liposome–GSN complexes

The cationic lipid, 1,2-dioleoyl-3-trimethylammonium-propane (DOTAP), was dissolved in chloroform and the solvent was evaporated under vacuum for 2 hours. The lipid film was hydrated with ultrapure water to a final lipid concentration of 1 mg $mL^{-1}$ and stored at 4 °C. Multilamellar liposomes were extruded with an Avanti mini-extruder (Avanti Polar Lipids, Alabaster, AL) (number of passages: 20 and polycarbonate filter size: 0.1 μm). Liposome-GSN complexes were obtained by mixing the liposomal dispersion with GSN for 15 minutes at 37° C at eight GSN/DOTAP weight ratios: 0.01, 0.05, 0.1, 0.2, 0.4, 1, 2, and 4.

### Preparation of liposome–protein complexes

Liposome–protein complexes were obtained by mixing the bare liposome or the liposome-GSN complexes with HP for 1 h at 37 °C (1 : 1 vol/vol).

### Dynamic light scattering and zeta potential

Preliminary characterization of the bare liposome, liposome–GSN, and liposome–protein complexes was performed by dynamic light scattering (DLS) and zeta-potential measurements using a Zetasizer Nano ZS (Malvern, UK). The results are given as the average value of three replicate experiments ± S.D.

### 1D SDS-PAGE experiments

Proteins were isolated from DOTAP and DOTAP-GSN by centrifugation at 18 620 rcf for 15 min at 4 °C using a Z 216 MK centrifuge (Hermle, Germany). Then we washed the pellets three times with PBS to eliminate unbound proteins and detach loosely bound proteins (the "soft corona"). The obtained pellets thus contained only tightly bound proteins, *i.e.*, the so-called "hard corona". Next, we suspended the pellets in 20 μL of Laemmli loading buffer, boiled them for 10 min, and again centrifuged at 18 620*g* for 15 minutes at 4 °C. Then supernatants were collected and diluted (1 : 5) before loading them on a stain-free gradient polyacrylamide gel (4–20% TGX precast gels, Bio-Rad) and run at 100 V for 120 min. Images were collected using a ChemiDoc™ gel imaging system (Bio-Rad, CA, USA) and processed using custom MatLab scripts (MathWorks, MA, USA). Briefly, protein patterns represent the intensity profiles of the image along the vertical lines corresponding to the samples. Further details of the image processing analysis for the determination of MW distributions can be found elsewhere.[54]

### Particle sequestration from the THP1 cell line

To investigate cellular uptake in the THP1 cell line, NBD-labeled liposomes (with HP or GSN) were administered to cells in a serum-free medium. THP1 cells were plated at 500 000 cells per mL in 12-well dishes and then incubated for different periods (30 s or 1, 2, or 3 h). After the treatment, the cells were washed with cold PBS and then run on a FACS Canto (BD Biosciences, San Jose, CA). The cells were gated using forward *versus* side scatter to exclude debris and then analyzed for the specific emission. The data were analyzed using FlowJo software (FlowJo LLC data analysis software, Ashland, OR, USA).

### Particle sequestration from circulating leukocytes

Peripheral whole blood was plated 120 μL per point and incubated for different periods (30 s or 5, 15, 30, or 60 min) at 37 °C with 6 μL of NBD-labeled liposomes-PC complexes (concentration of 1 μg $\mu L^{-1}$). We chose an NBD-labeling for its characteristic of intercalating within the lipid double layer in the hydrophobic core, thus without alteration in the formation of the protein corona. Sample dosing was performed using the lipid amount as a reference. The lipid amount is easily accessible as liposomal formulations were prepared at a fixed concentration of 1 mg $mL^{-1}$. After treatment, the cells were suspended in 2 ml of physiological solution and subjected to centrifugation. Red blood cells were then lysed with a buffer containing 155 mM $NH_4Cl$, 12 mM $NaHDO_3$, and 0.1 mM EDTA.

 

After washing twice with PBS by centrifugation to exclude the particles loosely associated, the cells were labelled with the following diluted antibodies: anti-CD3/BV510 (cat. 564713, dilution 1 : 50), CD56/BV421 (cat. 562751, dilution 1 : 50), anti-CD4/APC (cat.555349, dilution 1 : 10), anti-CD14/PerCP (cat. 340585, dilution 1 : 50), anti-CD45/allophycocyanin-H7 (cat. 560178, dilution 1 : 50), and anti-CD19/PE-Cy7 (cat. 557835, dilution 1 : 100), all from BD Bioscience (San Jose, CA). The fluorescence signal of internalized liposome-PC complexes was evaluated by immunofluorescence and FACS analyses using a FACSCanto and measured as the percentage of FITC-positive cells by gating on distinct leukocyte subpopulations as previously described.[11] A representative donor is shown (Fig. S2 in the ESI†). Data analysis was performed using FlowJo™ software, with results reported in Fig. 2 as the mean ± standard deviation of three healthy donors.

### Confocal imaging experiment

THP-1 cells were cultivated in 20% FBS, 2 mM L-glutamine, and 1× Pen/Strep RPMI 1640 medium (Gibco). THP-1 cells were grown in suspension in T75 or T25 flasks and split upon reaching an approximate density of 350.000 cells per mL. On the day of the experiment, approximately 100.000 cells were seeded on slide chambers (FaLDon) pre-treated with poly-L-lysin (Sigma), following the manufacturer's protocol, to facilitate cell adhesion. Three experimental conditions were tested: (i) cells treated with 6 μL of DOTAP-Texas Red (0.1 mg $mL^{-1}$) and (ii) cells treated with a mixture of 6 μL of DOTAP-Texas Red and 24 μL of gelsolin (Sigma Aldrich, USA) (protein concentration = 0.2 mg $ml^{-1}$) pre-incubated for 15 min at 37 °C; 2 hours after cell exposure, the cells were stained with Hoechst 33342 (TermoFisher) and then fixed with 4% PFA, following manufacturer's protocols. Fluorescence imaging experiments were performed using a Zeiss LSM 880 Airyscan confocal microscope equipped with a 63×, 1.4 NA, an oil immersion objective, and GaAsP detectors. A 4-channel imaging experiment was carried out in sequential mode to avoid cross-talk between the emission spectra of different fluorophores. The following experimental setting was used: DOTAP-Texas Red was excited at 561 nm and emission was collected in the 545–645 nm range, Hoechst was excited at 405 nm and emission was collected in the 410–445 nm range.

### TNFα production

Ficoll-Hypaque gradient centrifugation was used to isolate PBMCs from peripheral blood of healthy volunteers. The cells were plated at $1 \times 10^6$ cells per mL and incubated for 1 h at 37 °C with 10 μg $mL^{-1}$ NBD-labeled liposomes (with HP or GSN) in RPMI medium. After that, 10 μg $ml^{-1}$ brefeldin A (BFA) was added to the culture and left for an additional 3 h. The cells were harvested and first surface-stained with anti-CD14/V500 (cat. 562693, clone MφP9; BD Biosciences, San Jose, CA), subsequently fixed, permeabilized using BD Cytofix/Cytoperm and finally the cells were stained with anti-TNFα/APC (clone cA2, Miltenyi Biotec). Intracellular cytokine detection was evaluated by flow cytometry and measured as the percentage of TNFα positive cells by gating on $CD14^+$ monocyte population. Experiments were performed using a FACSCanto (BD Biosciences, San Jose, CA). Data analysis was performed using FlowJo™ software.

### Cell viability experiments

The cell viability of the THP-1 cell line was evaluated using 2,3-bis-(2-methoxy-4-nitro-5-sulfophenyl)-2*H*-tetrazolium-5-carboxanilide (XTT assay, cell proliferation Kit II, Roche). The cells were seeded on 96-well plates (50 000 cells per well) and incubated with an increasing amount of bare liposome (1, 2, 4, 6, 8, 10 and 12 μg) in RPMI-1640 (Gibco, Carlsbad, CA, USA) medium supplemented with 2 mM L-glutamine, 100 IU $mL^{-1}$ penicillin/streptomycin and 10% fetal bovine serum. Then, the cells were incubated for 48 h at 37 °C. Next, 50 μL of XTT solution, previously prepared as indicated in the kit protocol, was added to each well of the plate and the treated cells were incubated at 37 °C for 3 h. After that, the absorbance of each well was measured with a Glomax Discover System (Promega, Madison, WI, USA), a detection multi-mode instrument with high performance. All the measurements were made in triplicate.

### Minimum information reporting in the bio-nano experimental literature (MIRIBEL)

Accurate characterization in nanomedicine research is vital for generating reliable and reproducible results.[55] Among the possible options, the experimental details of this investigation were provided matching with the MIRIBEL reporting standard for bio-nano research.[56] All the information useful to replicate the experiments have been incorporated into a companion checklist (Table S2 in the ESI†).

### NF-kB luciferase reporter assay

TLR-specific activation assays were performed using human embryonic kidney 293 (HEK293) cells expressing luciferase under control of the NF-kB promoter and stably transfected with TLR2 or TLR4 purchased from InvivoGen (Toulouse, France). HEK293-transfected cells were maintained in DMEM supplemented with 4.5 g $L^{-1}$ glucose and 10% FBS, 1% penicillin/streptomycin solution (Invitrogen), 5 μg $mL^{-1}$ puromycin (Sigma-Aldrich, St Louis, MO) and 5 μg $mL^{-1}$ blasticidin (InvivoGen). For the NF-kB luciferase assay, 40 000 cells per well were seeded in 100 μL of complete DMEM without antibiotics in 96-well plates and incubated for 18 h at 37 °C. After this incubation, the medium was removed, the cells were washed with PBS, and 200 μL of DMEM without FBS were added. The cells were incubated with suitable amounts of DOTAP-HP or DOTAP-GSN and left for 5 h. As a positive control, specific TLR agonists were used (*i.e.*, 1 μM Pam3CSK4 and 10 μg $ml^{-1}$ LPS both from InvivoGen). After incubation, supernatants were collected from each well, the cells were washed with PBS and then lysed for 15 min at room temperature using 50 μL per well of 1 : 5 diluted "passive lysis buffer" (Promega, Madison WI). The protein concentration was evaluated by the Bio-Rad protein assay. In total, 3 μg of total pro-

teins for each sample were diluted in 50 μL of PBS, and 50 μL of luciferase assay substrate (Promega, Madison WI) was added. Emitted light was immediately quantified using a luminometer GloMax-Multi Detection System (Promega, Madison WI).

## Ethical statement

All experiments were performed in accordance with the institutional guidelines and approved by the ethics committee at the "Sapienza" University of Rome. Informed consent was obtained from the human participants of this study in accordance with the Declaration of Helsinki.

## Author contributions

Investigation: F. G., E. V., L. L., and G. F.; formal analysis: L. D. and E. V.; methodology: L. D.; software: L. D. and E. V.; conceptualization: F. C., D. P., A. Z., and G. C.; writing – original draft: F. G., L. D., F. C., A. Z., and G. C.; writing – review and editing: F. C., D. P., A. Z., and G. C; and supervision: A. Z. and G. C.

## Conflicts of interest

There are no conflicts to declare.

## Acknowledgements

When the work was conceived and performed LD was supported by a fellowship from the AIRC Foundation (ID 24143; 2019).

## References

1 A. Salvati, A. S. Pitek, M. P. Monopoli, K. Prapainop, F. B. Bombelli, D. R. Hristov, P. M. Kelly, C. Åberg, E. Mahon and K. A. Dawson, *Nat. Nanotechnol.*, 2013, **8**, 137–143.
2 J. L. Betker, D. Jones, C. R. Childs, K. M. Helm, K. Terrell, M. A. Nagel and T. J. Anchordoquy, *J. Controlled Release*, 2018, **286**, 85–93.
3 L. Digiacomo, D. Pozzi, S. Palchetti, A. Zingoni and G. Caracciolo, *Wiley Interdiscip. Rev.: Nanomed. Nanobiotechnol.*, 2020, e1615.
4 J. Park, D.-H. Lim, H.-J. Lim, T. Kwon, J.-S. Choi, S. Jeong, I.-H. Choi and J. Cheon, *Chem. Commun.*, 2011, **47**, 4382–4384.
5 M. Janát-Amsbury, A. Ray, C. Peterson and H. Ghandehari, *Eur. J. Pharm. Biopharm.*, 2011, **77**, 417–423.
6 S. Y. Shann, C. M. Lau, S. N. Thomas, W. G. Jerome, D. J. Maron, J. H. Dickerson, J. A. Hubbell and T. D. Giorgio, *Int. J. Nanomed.*, 2012, **7**, 799.
7 A. Chonn, P. Cullis and D. Devine, *J. Immunol.*, 1991, **146**, 4234–4241.
8 C. D. Walkey, J. B. Olsen, H. Guo, A. Emili and W. C. Chan, *J. Am. Chem. Soc.*, 2012, **134**, 2139–2147.
9 A. E. Nel, L. Mädler, D. Velegol, T. Xia, E. M. Hoek, P. Somasundaran, F. Klaessig, V. Castranova and M. Thompson, *Nat. Mater.*, 2009, **8**, 543–557.
10 Y. Qie, H. Yuan, C. A. Von Roemeling, Y. Chen, X. Liu, K. D. Shih, J. A. Knight, H. W. Tun, R. E. Wharen and W. Jiang, *Sci. Rep.*, 2016, **6**, 1–11.
11 C. Corbo, R. Molinaro, A. Parodi, N. E. Toledano Furman, F. Salvatore and E. Tasciotti, *Nanomedicine*, 2016, **11**, 81–100.
12 F. Giulimondi, L. Digiacomo, D. Pozzi, S. Palchetti, E. Vulpis, A. L. Capriotti, R. Z. Chiozzi, A. Laganà, H. Amenitsch and L. Masuelli, *Nat. Commun.*, 2019, **10**, 1–11.
13 G. Caracciolo, S. Palchetti, V. Colapicchioni, L. Digiacomo, D. Pozzi, A. L. Capriotti, G. La Barbera and A. Laganà, *Langmuir*, 2015, **31**, 10764–10773.
14 J. Simon, L. K. Müller, M. Kokkinopoulou, I. Lieberwirth, S. Morsbach, K. Landfester and V. Mailänder, *Nanoscale*, 2018, **10**, 10731–10739.
15 F. Chen, G. Wang, J. I. Griffin, B. Brenneman, N. K. Banda, V. M. Holers, D. S. Backos, L. Wu, S. M. Moghimi and D. Simberg, *Nat. Nanotechnol.*, 2017, **12**, 387.
16 M. Tonigold, J. Simon, D. Estupiñán, M. Kokkinopoulou, J. Reinholz, U. Kintzel, A. Kaltbeitzel, P. Renz, M. P. Domogalla and K. Steinbrink, *Nat. Nanotechnol.*, 2018, **13**, 862–869.
17 R. Dal Magro, B. Albertini, S. Beretta, R. Rigolio, E. Donzelli, A. Chiorazzi, M. Ricci, P. Blasi and G. Sancini, *Nanomedicine*, 2018, **14**, 429–438.
18 C. Astarita, S. Palchetti, M. Massaro-Giordano, M. Di Domenico, F. Petrillo, S. Boffo, G. Caracciolo and A. Giordano, *Pharmaceutics*, 2021, **13**, 867.
19 D. M. Smith, J. K. Simon and J. R. Baker Jr., *Nat. Rev. Immunol.*, 2013, **13**, 592–605.
20 T. Ishida, H. Harashima and H. Kiwada, *Curr. Drug Metab.*, 2001, **2**, 397–409.
21 J. Yang, A. Azuar, I. Toth and M. Skwarczynski, *Vaccine Design*, Springer, 2022, pp. 295–307.
22 C. R. Alving, *J. Immunol. Methods*, 1991, **140**, 1–13.
23 L. Raphael and B. Tom, *Clin. Exp. Immunol.*, 1984, **55**, 1.
24 D. Pozzi, G. Caracciolo, R. Caminiti, S. C. De Sanctis, H. Amenitsch, C. Marchini, M. Montani and A. Amici, *ACS Appl. Mater. Interfaces*, 2009, **1**, 2237–2249.
25 E. Piktel, U. Wnorowska, M. Cieśluk, P. Deptuła, S. V. Prasad, G. Król, B. Durnaś, A. Namiot, K. H. Markiewicz and K. Niemirowicz-Laskowska, *Int. J. Mol. Sci.*, 2020, **21**, 2551.
26 T. S. Cohen, R. Bucki, F. J. Byfield, N. J. Ciccarelli, B. Rosenberg, M. J. DiNubile, P. A. Janmey and S. S. Margulies, *Cytokine*, 2011, **54**, 235–238.

 

27 D. Sezen, A. M. Bongiovanni, S. Gelber, U. Perni, J. M. Hutson, D. Skupski and S. S. Witkin, *Am. J. Obstet. Gynecol.*, 2009, **200**, 191.

28 Z. Yang, T. T.-Y. Chiou, T. P. Stossel and L. Kobzik, *Am. J. Physiol.: Lung Cell. Mol. Physiol.*, 2015, **309**, L11–L16.

29 S. Berger, M. Berger, C. Bantz, M. Maskos and E. Wagner, *Biophys. Rev.*, 2022, **3**, 011303.

30 M. P. Monopoli, D. Walczyk, A. Campbell, G. Elia, I. Lynch, F. Baldelli Bombelli and K. A. Dawson, *J. Am. Chem. Soc.*, 2011, **133**, 2525–2534.

31 P. Jain, R. Pawar, R. Pandey, J. Madan, S. Pawar, P. Lakshmi and M. Sudheesh, *Biotechnol. Adv.*, 2017, **35**, 889–904.

32 M. H. Jazayeri, H. Amani, A. A. Pourfatollah, H. Pazoki-Toroudi and B. Sedighimoghaddam, *Sens. Bio-Sens. Res.*, 2016, **9**, 17–22.

33 L. Digiacomo, F. Giulimondi, A. L. Capriotti, S. Piovesana, C. M. Montone, R. Z. Chiozzi, A. Laganà, M. Mahmoudi, D. Pozzi and G. Caracciolo, *Nanoscale Adv.*, 2021, **3**, 3824–3834.

34 S. Zanganeh, G. Hutter, R. Spitler, O. Lenkov, M. Mahmoudi, A. Shaw, J. S. Pajarinen, H. Nejadnik, S. Goodman and M. Moseley, *Nat. Nanotechnol.*, 2016, **11**, 986–994.

35 S. M. Moghimi and A. C. Hunter, *Pharm. Res.*, 2001, **18**, 1–8.

36 J. Szebeni and S. M. Moghimi, *J. Liposome Res.*, 2009, **19**, 85–90.

37 S. M. Moghimi, D. Simberg, T. Skotland, A. Yaghmur and C. Hunter, *J. Pharmacol. Exp. Ther.*, 2019, **370**, 581–592.

38 Z. Liu, W. Jiang, J. Nam, J. J. Moon and B. Y. S. Kim, *Nano Lett.*, 2018, **18**, 6655–6659.

39 M. A. Miller, R. Chandra, M. F. Cuccarese, C. Pfirschke, C. Engblom, S. Stapleton, U. Adhikary, R. H. Kohler, J. F. Mohan and M. J. Pittet, *Sci. Transl. Med.*, 2017, **9**, eaal0225.

40 W. Chanput, J. Mes, R. A. Vreeburg, H. F. Savelkoul and H. J. Wichers, *Food Funct.*, 2010, **1**, 254–261.

41 K. Kristensen, A. J. Urquhart, E. Thormann and T. L. Andresen, *Nanoscale*, 2016, **8**, 19726–19736.

42 A. Jhaveri, P. Deshpande, B. Pattni and V. Torchilin, *J. Controlled Release*, 2018, **277**, 89–101.

43 C. D. Walkey, J. B. Olsen, F. Song, R. Liu, H. Guo, D. W. H. Olsen, Y. Cohen, A. Emili and W. C. Chan, *ACS Nano*, 2014, **8**, 2439–2455.

44 G. Caracciolo, *Nanomedicine*, 2015, **11**, 543–557.

45 R. Liu, W. Jiang, C. D. Walkey, W. C. Chan and Y. Cohen, *Nanoscale*, 2015, **7**, 9664–9675.

46 A. Bigdeli, S. Palchetti, D. Pozzi, M. R. Hormozi-Nezhad, F. Baldelli Bombelli, G. Caracciolo and M. Mahmoudi, *ACS Nano*, 2016, **10**, 3723–3737.

47 S. Palchetti, L. Digiacomo, D. Pozzi, G. Peruzzi, E. Micarelli, M. Mahmoudi and G. Caracciolo, *Nanoscale*, 2016, **8**, 12755–12763.

48 C. D. Walkey and W. C. W. Chan, *Chem. Soc. Rev.*, 2012, **41**, 2780–2799.

49 F. Bordi, S. Sennato and D. Truzzolillo, *J. Phys.: Condens. Matter*, 2009, **21**, 203102.

50 G. Caracciolo, D. Pozzi, A. L. Capriotti, C. Cavaliere, P. Foglia, H. Amenitsch and A. Laganà, *Langmuir*, 2011, **27**, 15048–15053.

51 E. Vulpis, F. Cecere, R. Molfetta, A. Soriani, C. Fionda, G. Peruzzi, G. Caracciolo, S. Palchetti, L. Masuelli and L. Simonelli, *OncoImmunology*, 2017, **6**, e1279372.

52 Y. Cheng, X. Hu, C. Liu, M. Chen, J. Wang, M. Wang, F. Gao, J. Han, D. Sun and C. Zhang, *Cell. Physiol. Biochem.*, 2017, **41**, 205–212.

53 A. Asea, M. Rehli, E. Kabingu, J. A. Boch, O. Baré, P. E. Auron, M. A. Stevenson and S. K. Calderwood, *J. Biol. Chem.*, 2002, **277**, 15028–15034.

54 L. Digiacomo, S. Palchetti, F. Giulimondi, D. Pozzi, R. Z. Chiozzi, A. L. Capriotti, A. Laganà and G. Caracciolo, *Lab Chip*, 2019, **19**, 2557–2567.

55 M. Mahmoudi, *Nat. Commun.*, 2021, **12**, 1–5.

56 M. Faria, M. Björnmalm, K. J. Thurecht, S. J. Kent, R. G. Parton, M. Kavallaris, A. P. Johnston, J. J. Gooding, S. R. Corrie and B. J. Boyd, *Nat. Nanotechnol.*, 2018, **13**, 777–785.